JOURNAL OF GEOPHYSICAL RESEARCH, VOL. 88, NO. C10, PAGES 5925–5938, JULY 20, 1983

Transformation of Wave Height Distribution

EDWARD B. THORNTON

Naval Postgraduate School, Monterey, California 93940

R. T. GUZA

Shore Processes Laboratory, Scripps Institution of Oceanography, University of California La Jolla, California 92093

The transformation of random wave heights during shoaling, including waves breaking in the surf zone, was measured with an extensive array of instruments in the field. The initially Rayleigh height distributions in 10-m depth were observed to be modified by shoaling and breaking into new distributions which are again nearly Rayleigh but with some energy loss. Using locally measured H_{rms}, the Rayleigh distribution describes the measured central moments of $H_{1/3}$ and $H_{1/10}$ with average errors of -0.2% and -1.8%, respectively. The Rayleigh distribution is used to describe the random nature of wave heights in a single-parameter transformation model based on energy flux balance. The energy losses associated with wave breaking are parameterized using observed breaking wave distributions coupled with a periodic bore dissipation model. Using incident waves measured in 10-m depth as input conditions, the model predicts H_{rms} at shoreward locations within a rms error of $\pm 9\%$. The single free parameter of the model, a constant B representing the fraction of foam on the face of a wave, was chosen to best fit the data. The resulting large value of B implies that the simple periodic bore dissipation function substantially underestimates the actual dissipation.

1. INTRODUCTION

As waves approach the breakpoint, wave-induced velocities increase and dissipation due to the bottom friction and/or percolation becomes increasingly important. But once the waves start to break, turbulent dissipation of the wave energy is the dominant dissipative mechanism, and breaking processes dominate the wave transformation. In contrast to monochromatic waves, there is no well-defined breakpoint for random waves. The largest waves tend to break farthest offshore and small waves closer to shore. At each spatial point there are both broken and unbroken waves (sometimes having the same height), and the percentage of broken waves varies as a function of position.

Most nearshore dynamical models for longshore currents, rip currents, and flow over irregular bottom describe the waves as monochromatic and of constant amplitude at each location. An improvement in these models would be to more realistically include the random nature of the waves. The objective of this paper is to characterize the transformation of the wave height probability density function (pdf) from offshore to the shoreline with a simple model as a first step in the evolution of dynamical models having a probabilistic description for waves. Both analytical and numerical models are developed for describing the transformation of wave heights. The models are compared with results from random wave experiments in the laboratory and from an extensive set of field measurements.

Earlier models of random wave transformation are reviewed in the first section. Then the transformation of waves, including dissipation due to breaking and bottom friction, is described by an energy flux balance model. The wave height pdf of all waves (broken and unbroken) is shown by the field data to be well described by the Rayleigh distribution everywhere. The observed distributions of breaking and broken wave heights are fitted to simple analytical forms, and breaking wave dissipation is calculated by using a periodic bore formulation. The energy flux equation is integrated to yield local values of H_{rms} as a function of offshore wave conditions. Both analytical and numerical models are developed. In the last section the models are compared with results from random wave experiments in the laboratory and from an extensive set of field measurements.

Paper number 3C0515.
0148-0227/83/003C-0515$05.00

2. EXISTING RANDOM WAVE TRANSFORMATION MODELS

There are two generic classes of random wave shoaling and breaking models. The earlier models [*Collins*, 1970; *Battjes*, 1972; *Kuo and Kuo*, 1974; *Goda*, 1975] describe shoaling as only dependent on the 'local' water depth and are described here first. A second type of model is based on integrating the energy flux balance equation with wave height dependent on the shoaling processes along the integral path starting in deep water [*Battjes and Janssen*, 1978] and will be further refined and developed in this paper.

Wave heights are described, in general, by a joint distribution of height and frequency (or period or wave number, equivalently). To simplify the analysis, all the above authors assume the waves are very narrow banded in frequency and coming from the same direction, such that all wave heights of the distribution are associated with an average frequency $\bar{f}$ and mean direction $\bar{\theta}$. Therefore, starting in deep water, the waves are described by the single-parameter Rayleigh pdf with the implied assumptions of a narrowband Gaussian process.

In the local models, the deep water wave heights are first transformed into shallow water using shoaling theory in which all energy losses are neglected. The shoaled unbroken wave height distribution is calculated locally using

$$p(H) = \frac{2H}{(K_s H_d)^2} \exp\left[-\left(\frac{H}{K_s H_d}\right)^2\right] \tag{1}$$

where K_s is a shoaling coefficient and H_d is the deepwater rms wave height. Eventually, the waves reach such shallow water that they start to break, with the largest waves breaking far-

TABLE 1. Modified Probability Density Functions Due to Wave Breaking

AUTHOR	DISTRIBUTION	SHOALING	BREAKER CRITERIA
COLLINS (1970)	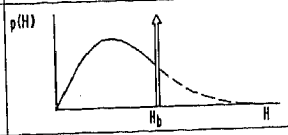	LINEAR	$\frac{H_b}{H_d} = 0.76\beta^{1/7}(H_d/L_d)^{-1/4}$ (AFTER LeMEHAUTE AND KOH, 1967)
BATTJES (1972)	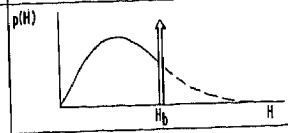	LINEAR	$H_b = \frac{0.88}{k}\,\mathrm{TANH}\left(\frac{\gamma}{0.88}kh\right)$
KUO and KUO (1974)	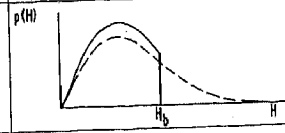	LINEAR	$H_b = 0.63h$
GODA (1975)	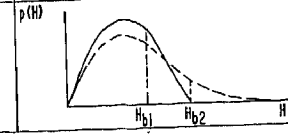	NONLINEAR (SHUTO, 1974)	$\frac{H_b}{H_d} = A\frac{L_d}{H_d}\left\{1-\exp\left\{-1.5\frac{h}{H_d}\frac{H_d}{L_d}(1+K\tan\beta)^P\right\}\right\}$ (AFTER GODA, 1975)

The dotted lines represent the original Rayleigh distributions and the heavy lines represent the modified distributions.

thest offshore. Wave breaking is simulated by truncating the tail of the Rayleigh distribution based on various breaker criteria where, in general, $H_b = H_b(h, H_d, \bar{f}, \beta)$ where h is the local water depth and $\tan\beta$ is the bottom slope.

Collins [1970] and *Battjes* [1972] used a sharp cutoff of the Rayleigh pdf with all waves that are breaking or have already broken having heights equal to H_b. Requiring all the broken waves to have the same height H_b results in a delta function at H_b in the pdf (see Table 1). Collins used linear shoaling theory and the breaking criterion after *LeMehauté and Koh* [1967]. *Battjes* [1972] also used linear theory to shoal the waves and applied the breaking criterion based on *Miche*'s [1954] formula for the maximum height of periodic waves of constant form:

$$H_b = \frac{0.88}{k}\tanh\left(\frac{\gamma}{0.88}kh\right) \tag{2}$$

where γ is an adjustable coefficient. In shallow water, (2) simply reduces to

$$H_b = \gamma h \tag{3}$$

Kuo and Kuo [1974] modeled the effect of breaking on wave statistics by using a sharply truncated conditional Rayleigh pdf with the breaking wave height simply proportional to local water depth (3). They assumed the waves generally have some height smaller than H_b after breaking and redistributed the broken waves across the range of heights in proportion to the probability of unbroken waves at each height. Stated in terms of the conditional wave height pdf,

$$p(H) = p(H/0 \le H \le H_b) = p_0(H)\left[\int_0^{H_b} p_0(H)\,dH\right]^{-1}$$

$$= 0 \qquad H > H_b, \tag{4}$$

where $p_0(H)$ is the pdf prior to truncation; $p(H)$ is simply a truncated Rayleigh distribution renormalized to unity. Table 1 shows the original Rayleigh distribution with dotted lines and the truncated, renormalized Rayleigh distribution (4) in solid lines. The distribution by Kuo and Kuo is more realistic (as will be seen later) in that the delta function at a particular breaking wave height [*Collins*, 1970; *Battjes*, 1972] is removed, but the sharp cutoff at H_b is still nonphysical.

Goda [1975] assumed that wave breaking occurs with linearly varying probability over a range of wave heights, resulting in a modified distribution with a gradual cutoff of the distribution around H_b (Table 1). The spreading of breakers over a range of heights crudely compensates for the simplification of using a single wave period in the breaker height criterion and is certainly more realistic than models which assert that breakers are all the same height. *Goda* [1975] used a breaker criterion based on laboratory data which takes into account bottom slope and wave steepness in deep water H_d/L_d [*Goda*, 1970] and calculated the wave shoaling using the monochromatic nonlinear theory of *Shuto* [1974]. We note that the use of monochromatic, nonlinear theories to shoal random waves (which have been characterized by a single frequency) is theoretically unjustifiable and introduces unnecessary numerical complications into already relatively crude models.

The common idea of these studies is to cut off the portion of the wave height pdf beyond a breaker height, which is controlled by the water depth and other factors. The methods differ in the techniques of cutoff and the formulae used to define breaker heights. A shortcoming of these earlier models is that the calculated wave heights depend only on the local depth. In application to cases where the depth is not monotonically decreasing, such as a barred coast, the predicted wave heights decrease over the bar due to breaking and then increase in the deeper trough, simply following the local depth. The increase in wave height in the trough indicates a generation of energy which is physically inappropriate.

Models applying the energy flux balance [*Battjes and Janssen*, 1978] to calculate wave heights can properly predict shoaling of waves over nonmonotonic bottom profiles. For simplicity, Battjes and Janssen considered only waves normally incident to a coastline with straight and parallel contours, so that

$$\frac{\partial EC_g}{\partial x} = \langle \varepsilon \rangle \tag{5}$$

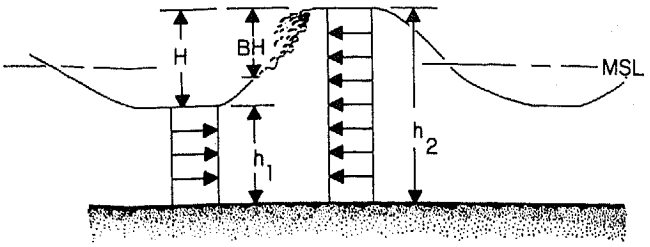

Fig. 1. Periodic bore used to describe spilling breakers.

where E is the energy density, C_g is the group velocity, x is the onshore coordinate, and $\langle\varepsilon\rangle$ is the average dissipation per unit area. The energy density and group velocity are given by using linear theory relationships. Specification of the dissipation term requires consideration of breaking wave dynamics.

In general, wave breaking occurs as a result of kinematic instability as the fluid velocity at the creast exceeds the wave speed, resulting in the crest curling over and injecting fluid at the surface. Dissipation rates and depth of turbulent penetration are dependent on the strength and size of vortices generated at the surface, which vary with the breaker type [*Miller*, 1976]. Turbulence can penetrate to the bottom under plunging breakers. For spilling breakers the turbulence is confined to a surface layer, primarily between the crest-trough region which at least qualitatively resembles the processes of a bore. For this reason the rate of energy dissipation due to shallow water wave breaking is usually modeled after a bore, an approach originally suggested by LeMehauté [1962]. The details of the turbulence dynamics in the bore (spilling breaker) is avoided by applying conservation of mass and momentum at regions of uniform flow upstream and downstream of the bore (Figure 1). The average rate of energy dissipation per unit area is calculated [*Stoker*, 1957]:

$$\varepsilon_{\text{bore}} = \frac{1}{4}\rho g \frac{(h_2 - h_1)3}{h_1 h_2} Q \simeq \frac{1}{4}\rho g \frac{(BH)^3}{h^2} Q \tag{6}$$

where the wave height H is measured as the maximum to minimum of the bore, Q is the volume discharge per unit area across the bore, and B is a breaker coefficient of 0(1). The coefficient B accounts for the differences in various breaker types and is considered as a function of the proportion of the foam region on the face of the breaker. The coefficient B will be the only unspecified parameter in the model and will be determined from the data.

Various formulations have been suggested for the bore discharge Q in (6). The simplest description of Q for waves is for a linear periodic bore [*Hwang and Divoky*, 1970]:

$$Q = \frac{Ch}{L} \tag{7}$$

where C is the wave speed and L is the wave length. The bore dissipation function is used to describe only the breaking waves of the random wave distribution.

Battjes and Janssen [1978] use the dissipation function (6) with (7), but they reduce the dependence on the depth by assuming that $H/h = 0(1) = 1$. They specify the percent of breaking waves at a particular location as simply the area under the delta function at H_b of the truncated Rayleigh wave height pdf. The dissipation function applied to the broken waves is substituted into the energy flux equation (5) which is numerically integrated. Good comparisons were obtained between calculated rms wave heights and laboratory measurements, even for a barred beach. A deficiency of the Battjes and Janssen model is that the wave height distribution, although conceptually simple, is not a good representation of the measured wave height pdf because of the delta function and truncation at H_b. The agreement between calculated and observed H_{rms} does not mean that the underlying pdf's are similar, as Battjes and Janssen noted.

3. Transformation of Wave Height Distribution Model

The model developed here describes the transformation of the wave height distribution. The model is similar in concept to that of *Battjes and Janssen* [1978], but it is extended to describe realistically the transformation of wave height pdf's as well as H_{rms}. In addition, bottom friction is considered in the dissipation function. For straight and parallel contours the average energy flux balance, including bore $\langle\varepsilon_b\rangle$ and frictional dissipation $\langle\varepsilon_f\rangle$, is given by

$$\frac{\partial E\, C_{gx}}{\partial x} = \langle\varepsilon_b\rangle + \langle\varepsilon_f\rangle \tag{8}$$

where C_{gx} is the x component of the group velocity.

The total energy flux in (8) is properly described by using an energy density spectrum with group velocities integrated over all frequencies and directions. Unfortunately, there is little theoretical guidance concerning how to calculate energy fluxes for a broad-banded (in direction and frequency) nonlinear wave field with some wave breaking. *Thornton and Guza* [1982] showed, for this same field data set, that the waves shoreward of 4 m depth can be frequency non-dispersive across the sea swell frequency range with phase speeds approximately given by $\sqrt{gh}$, which is the same as the linear phase speed at the spectral peak. These measurements suggest using a lowest order model for the energy density and group velocity given by the linear wave theory relationships

$$E = \frac{1}{8}\rho g H_{\text{rms}}{}^2 = \frac{1}{8}\rho g \int_0^\infty H^2 p(H)\, dH \tag{9}$$

$$C_{gx} = \frac{C}{2}\left(1 + \frac{2kh}{\sinh 2kh}\right)\cos\bar{\theta} \tag{10}$$

where $\bar{\theta}$ is the mean wave direction and k is the wave number associated with average frequency $\bar{f}$ corresponding to the peak of the spectrum. Although this crude representation may not be theoretically justified, similar quasilinear approximations have yielded remarkably accurate models for set-up [*Bowen et al.*, 1968; *Battjes and Janssen*, 1978].

At this point, we have the governing energy flux relation (8), with the dependence of EC_{gx} on H_{rms} and h given by (9) and (10). The dissipation rate (ε_b) as a function of H and h, for a wave known to be breaking, is given by (6) with the bore discharge described by (7). In the following sections, we complete the determination of ε_b by specifying the pdf of wave heights and the probability that a wave of a given height will be breaking. Equation (8) can then be integrated and the resulting H_{rms} compared with observations.

3.1. *Wave Height Distributions*

The Rayleigh wave height distribution was shown by *Longuet-Higgins* [1952] to apply to deep water waves on the assumption that the sea waves are a narrow-banded, linear

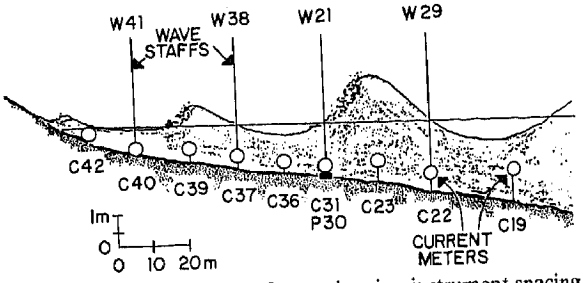

Fig. 2. Cross section of surf zone showing instrument spacing and elevations relative to measured waves on November 20, 1978 at Torrey Pines Beach, California.

Gaussian process. The Rayleigh wave height probability density function is

$$p(H) = \frac{2H}{H_{\text{rms}}^2} \exp\left[-\left(\frac{H}{H_{\text{rms}}}\right)^2\right] \tag{11}$$

which is entirely specified by H_{rms}. The Rayleigh distribution is applied correctly only to linear waves [*Longuet-Higgins*, 1975]. The distribution derived with a linear assumption would not be expected to hold for waves approaching maximum height, i.e., close to breaking, as in the surf region or for broader-banded 'sea' conditions with whitecaps.

The theoretical Rayleigh distribution has been found by several authors [*Chakrabarti and Cooley*, 1977; *Forristal*, 1978] to overpredict the number of large waves in the tail compared with observations. Various explanations including nonlinearity [*Forristal*, 1978; *Tayfun*, 1980; *Longuet-Higgins*, 1980], whitecapping [*Tayfun*, 1981], and finite bandwidth [*Longuet-Higgins*, 1980] have been examined as causes for the deviation from a Rayleigh distribution. *Tayfun*'s [1981] breaking effect and *Longuet-Higgins'* [1980] finite bandwidth mechanism both have some success in explaining field data. These studies seek to explain deviations from a Rayleigh distribution, but the relevant point here is that wave heights appear to be nearly Rayleigh under a much wider range of conditions than the strict assumptions of a narrow band Gaussian (linear) process would imply. We now describe some field experiments and show that wave height data even within the surf zone are reasonably well described by the Rayleigh distribution.

3.2. *Field Data Analysis*

Experiments measuring wave transformation were conducted at Torrey Pines Beach, California, during November 1978. The details and various results of the experiments have been described by *Guza and Thornton* [1980; 1981], *Huntley et al.* [1981], and *Thornton and Guza* [1982]. The beach is gently sloping and composed of moderately sorted, fine-grained sand. The beach profile shows no well-developed bar structure and is remarkably free from longshore topographic inhomogeneities. An extensive array of instruments was deployed to study nearshore wave dynamics. Measurements described here are from sensors located along an on-offshore transect from 10-m depth to the inner surf zone. A cross section of a typical instrument transect inside 3-m depth is shown in Figure 2. The waves have been drawn to scale (vertical scale distorted 1:20), and they show the horizontal wavelengths of dominant 14-second period swell as spatially well resolved. The sensors used here consisted of 11, two-axis Marsh-McBirney electromagnetic current meters (denoted by C), four Stathem temperature compensated pressure transducers (P), and four dual-resistance wire wave staffs (W). The shoreline and mean breaker positions were very much a function of the tidal stage (mean range 1.5 m). Instruments inshore of C22 were uncovered at spring low tides and all instruments were immersed at neap high tides.

During the experiments, significant offshore wave heights varied between 60 and 160 cm. The average peak frequency of the incident wave spectra varied little during the experiments and was about 0.07 Hz. Shadowing by offshore islands and offshore refraction limit the angles of wave incidence in 10-m depth to less than 15° [*Pawka et al.*, 1976]. The condition of nearly normally incident spilling (or mixed plunging-spilling) waves, breaking in a continuous way across the surf zone, prevailed during most of the experiments. Winds during the experiments were generally light and variable in direction.

Wave heights were determined from the surface elevation records using the 'zero-up-crossing method,' in which the wave height is defined as the difference of the maximum and minimum occurring between two consecutive zero-up crossings. The results using this method are very sensitive to the definition of mean level about which the zero-up crossings are computed and to high-frequency noise. In extreme cases, very low-frequency signals, such as the rise or fall of the tides or surf beat, can cause the troughs of the waves to be above the calculated 'average' water level. It is important to define the mean water level over a time scale which is of the order of only a few waves if the interest is the height statistics of sea and swell. Therefore the data were first linearly detrended to exclude effects of the rising and falling of the tides and then high-pass filtered with a cutoff frequency of 0.05 Hz (20-s period) to exclude surf beat. High-frequency signals, either artificial (e.g., electrical noise) or high-frequency capillary waves, can result in an increase in the zero-up crossings as the sea swell waves cross through zero, with a concomitant increase in the number of waves counted. Therefore the data were also low pass filtered with a high frequency cutoff (0.3 or 0.5 Hz) depending on sensor type and depth, as discussed below. Note that the choice of the range of frequencies examined will affect the results and leads to some subjectivity.

The filtering was accomplished by Fourier transforming the signals, zeroing out the Fourier amplitude coefficients in the filtered-out frequencies, and inverse transforming the complex spectrum to obtain the filtered time series. The entire 68-minute record was transformed at one time to minimize the end effects which result in spectral leakage and to obtain maximum resolution giving very sharp roll-off at the filter cutoffs.

Since the average wave period was about 14 s, the total number of waves in the 68-minute record was about 300. Empirical probability density functions and height statistics of root mean square wave height H_{rms}, significant wave height, $\bar{H}_{1/3}$ (average of the heights of the $\frac{1}{3}$ highest waves), $\bar{H}_{1/10}$ (average of the heights of the $\frac{1}{10}$ highest waves), and $H_{\max}$ were calculated from the ordered set of wave heights.

To take advantage of the large number of current meters, current data were used with linear theory to infer wave heights. The rationale for transforming the velocities to infer surface elevation is based on the earlier work of *Guza and Thornton* [1980]. By intercomparing wave staffs and other sensors they showed, for this same data set, that linear theory spectral transformations could be used to calculate surface elevation standard deviations either from pressure meters or current meters at the same horizontal location with less than a 20% error and, typically, less than 10%.

To obtain elevation time series from current measurements, the complex Fourier spectra of the horizontal velocity components $U(f)$, $V(f)$ were first calculated and vectorially added.

TABLE 2. Wave Conditions Offshore and Breaker Type

Date	rms Wave Height H_0, cm	$\bar{f}$, Hz	Depth, cm	Spectral Width ζ	Breaker Type
Nov. 4	35	0.063	1069	0.66	spill
Nov. 10	56	0.055	1072	0.72	spill
Nov. 12	88	0.077	1088	0.57	spill
Nov. 17	38	0.069	1053	0.63	spill/plunge
Nov. 18	49	0.069	1050	0.51	spill/plunge
Nov. 20	50	0.063	1022	0.76	plunge

The complex surface elevation spectrum $X(f)$ was calculated applying the linear wave theory transfer function $\mathbf{H}(f)$:

$$X(f) = \mathbf{H}(f) \cdot \mathbf{V}(f) \tag{12}$$

Only the sea swell band of frequencies is considered, so that the wave approach is almost normal to shore. Therefore it is assumed in the vector addition that $U(f) \gg V(f)$, and the phase of the surface elevation is associated with the phase of $U(f)$ only. It is assumed that wave reflection is negligible. The complex surface elevation spectrum was then inverse transformed to obtain the surface elevation time series from which the wave height distribution was calculated. Surface elevations were also inferred from pressure signals by transforming the pressure records using linear theory. With increasing frequency and depth, the signal to noise ratio of the surface wave-induced velocity and pressure signals decreases due to hydrodynamic filtering. Simultaneously, the spectral transfer functions $H(f)$ for both velocity and pressure exponentially increase. Therefore the surface elevation spectra obtained from pressure and current meter data first decrease in energy density from the peak frequency to higher frequencies, but 'turn up' at high frequencies (e.g., above 0.3 Hz for pressure signals measured in 10-m depth). The turn up is due to noise being amplified by the exponentially increasing transfer function $H(f)$. Thus the high-frequency filter cutoff was set at the frequency at which the inferred surface elevation spectrum turns up, which varied with depth; the signals measured using deeper instruments had to be more severely filtered ($\sim$0.3 Hz for 10-m-depth instruments) than shallow water instruments. A high frequency cutoff of 0.5 Hz was applied to all instruments shallower than about 3-m depth for H_{rms} calculations.

3.3. *Comparison with Rayleigh Distribution*

Six days were selected for analysis covering a wide range of conditions (see Table 2). Empirical pdf's of wave heights derived from velocity and pressure measurements are compared with the Rayleigh pdf for selected depths on November 20 (Figure 3). The Rayleigh pdf depends only on the local H_{rms}. Since H_{rms} first increases towards the mean breaker point and then decreases, the mode and apparent width of the Rayleigh pdf first increases and then decreases when plotted against H/H_0 (Figure 3). The width of 'bins' used is the same constant fraction of local H_{rms} for all empirical pdf's, so that as H_{rms} decreases, the width of the bins of the pdf's in Figure 3 narrows. The Rayleigh pdf appears to qualitatively describe the measured wave heights everywhere. The largest discrepancies of the measured waves with the Rayleigh pdf are deficits at the lowest and highest waves. But the bulk of the distribution is reasonably well predicted, and therefore the central moments such as $\bar{H}$ and H_{rms} should be well predicted using the Rayleigh pdf for model comparisons. Part of the reason for the deficit of higher wave heights (Figure 3) is because the wave heights inferred using current meters are low pass filtered with the high-frequency cutoff at 0.5 Hz, which has the effect of rounding off the peaks of the waves.

Directly measured wave heights using wave staffs compare slightly better with the Rayleigh distribution. For model comparisons of observed and predicted H_{rms} described later, the wave staffs were low-pass filtered with a high frequency cutoff at 0.5 Hz to be consistent with the other sensors. But for comparisons here with Rayleigh statistics, the wave staff measurements were low-pass filtered with a higher high-frequency cutoff of 1 Hz in order to minimize filtering affects. The wave staffs were usually located around the mean breaker point and within the surf zone. The wave staff measurements give a most severe test of the necessity to satisfy the strict theoretical requirements of linearity and narrow bandedness for the Rayleigh distribution to be applicable.

Table 2 gives offshore conditions of rms wave height H_0, $\bar{f}$, spectral width ξ at depth h, and the breaker type during each experiment. The spectral width parameter is given by [*Cartwright and Longuet-Higgins*, 1956]

$$\zeta^2 = \frac{m_0 m_4 - m_2^2}{m_0 m_4} \tag{13}$$

where m_n are the various spectral moments. A value of ζ near 1 is supposed to imply broad band waves, whereas a value $\zeta \to 0$ implies narrow-band waves. The Rayleigh distribution theoretically applies only for the case $\zeta \to 0$. Judging from the calculated ζ, the waves on all days were broad banded. To the contrary, visual observations indicated the waves on the 20th, for instance, were very narrow banded. The narrow bandedness was indicated by long-crested swell conditions and by the classical 'groupiness,' or beating, of the narrow-banded waves. The groupiness was exhibited by the waves at breaking going every several minutes from 2-m heights to essentially calm conditions and back again to 2-m waves at the arrival of another group of waves. The spectral width parameter, as defined, does not appear to be a good indicator of band width for shallow water waves, which are at least weakly nonlinear, as indicated by the presence of spectral harmonics. In fact, the spectra for November 20 [see *Guza and Thornton*, 1980] show a narrow swell peak and clear harmonic peaks at twice and three times the swell frequency. The definition of ζ does not distinguish free high-frequency waves (say, chop from local winds), which indicate true broadbandedness, from harmonic peaks which can be a consequence of the nonlinearity of a very narrow, energetic swell peak.

The cumulative exceedance of wave height distributions normalized by H_{rms} were calculated for wave staff measurements on November 4 (Figure 4). The waves on November 4 were relatively narrow band. The cumulative exceedance distri-

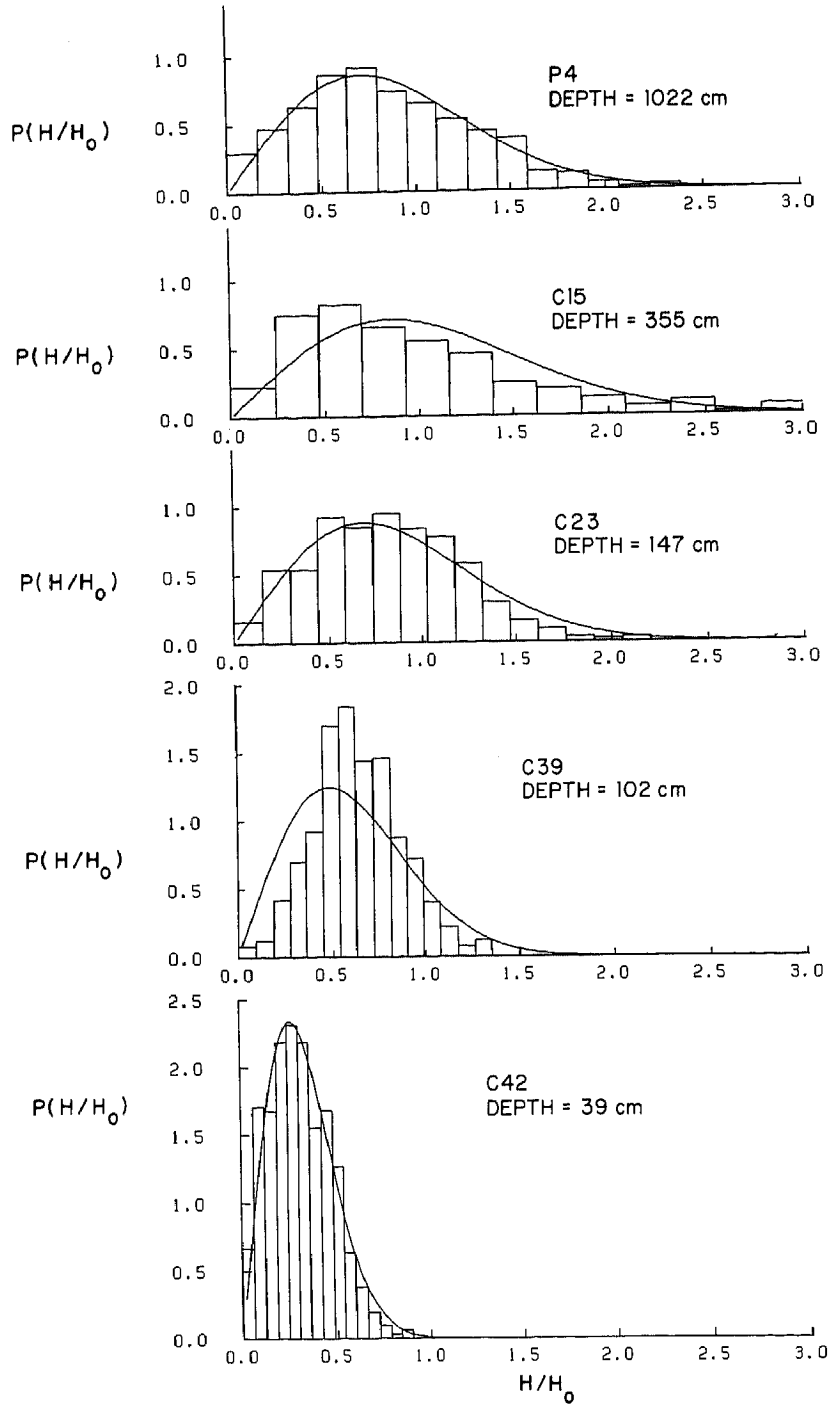

Fig. 3. Empirical probability density functions using pressure and current meters plotted against Rayleigh pdf for November 20, 1978. H_0 is H_{rms} in ~10-m depth = 50 cm.

bution emphasizes information in the high wave tail of the distribution. The mean breaker line for these measurements was between W29 and W21 so that W29 was just outside the surf zone and the others were inside. Note that the differences with the Rayleigh (solid line) are exaggerated in the tail for this kind of plot. The largest waves of the W29 distribution, measured just outside the surf zone, actually exceed the Rayleigh.

For wave staffs on all 6 days, measured H_{rms} and its approximation $H_{rms} = \sqrt{8m_0}$, where m_0 is the surface elevation variance, are compared in Figure 5. A 45° solid line is drawn to show a perfect correlation. The calculated correlation coefficient between the two variables is 0.995. The linear regression curve forced through zero is drawn as a dashed line, but can not be differentiated from the 45° line. The difference between the slopes of the 45° line and the regression line is the mean error over the range of measurements, which is +0.3%.

Measured $H_{1/3}$ (average of the highest one third waves), $H_{1/10}$, and H_{max} are compared with their respective Rayleigh-derived statistics in Figures 6–8, where for the Rayleigh distribution

$$H_{1/3} = 1.42\ H_{rms} \tag{14}$$

$$H_{1/10} = 1.56\ H_{rms} \tag{15}$$

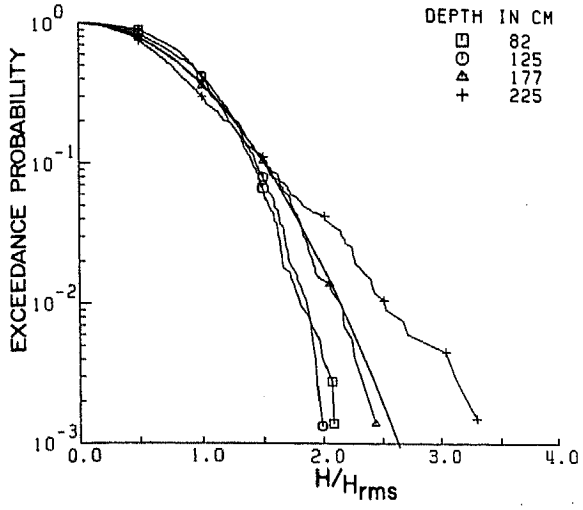

Fig. 4. Cumulative exceedence probability for wave staff measurements plotted against Rayleigh pdf for November 4, 1978.

The maximum wave height for the Rayleigh pdf was calculated by using [*Cartwright and Longuet-Higgins*, 1956]

$$H_{max} = [(\ln N)^{1/2} + 0.2886\,(\ln N)^{-1/2}]H_{rms} \qquad (16)$$

where N is the total number of waves in the distribution. The correlation coefficients were 0.997, 0.988, and 0.924 for $H_{1/3}$, $H_{1/10}$, and H_{max}, respectively. The linear regression curves forced through zero give an average percent error of -0.2%, -1.8%, and -6.8% for $H_{1/3}$, $H_{1/10}$, and H_{max}, respectively. The increasing spread of the points going from $H_{1/3}$ to $H_{1/10}$ to H_{max} may be because fewer points are used to calculate the statistic, H_{max} being the extreme with only one point used to calculate it. The heights may also be non-Rayleigh in the extreme tail. The results show that the central moments of H_{rms}, $H_{1/3}$, and even $H_{1/10}$ are well predicted by using the Rayleigh distribution. Therefore it is concluded that the Rayleigh distribution can be used to give a reasonable description of waves even in the surf zone, at least for the spilling breakers measured at Torrey Pines Beach.

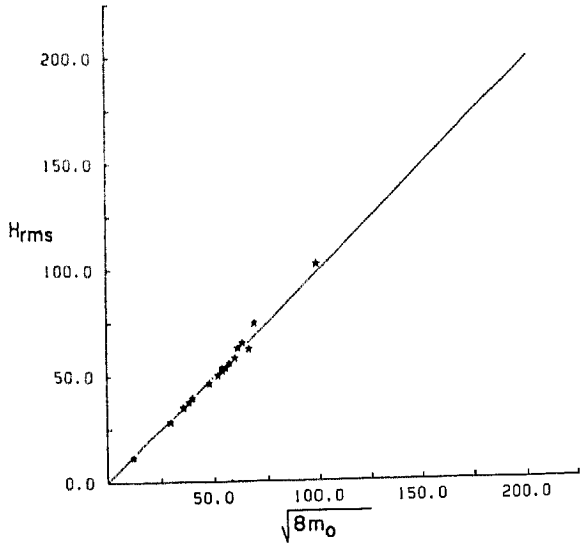

Fig. 5. Measured H_{rms} plotted against the approximation $H_{rms} = \sqrt{8m_0}$.

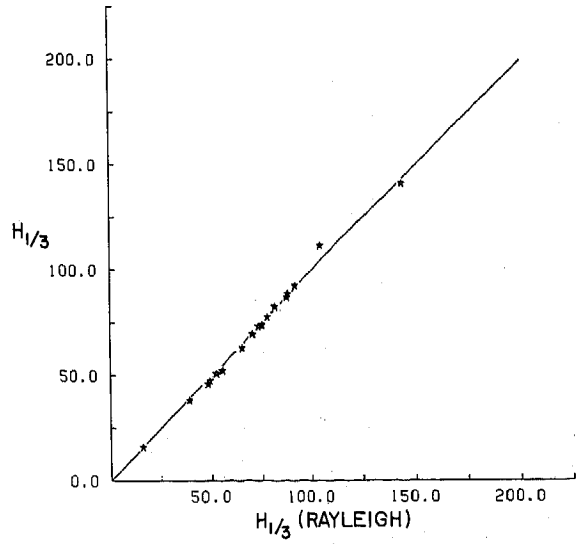

Fig. 6. Measured $H_{1/3}$ plotted against Rayleigh statistic $H_{1/3}$.

3.4. *Breaking Wave Height Distributions*

The observations clearly support use of the Rayleigh distribution as a good model for the wave height pdf. However, in order to calculate the breaking wave dissipation (ε_b), necessary for integration of the energy balance equation (8), we must specify which waves are breaking. Unfortunately, the importance of measuring the breaking wave distribution was not recognized until after the Torrey Pines experiment. Thus additional measurements were made at Soldiers Beach, Monterey, California to obtain the necessary breaking wave distributions.

The profile at Soldiers Beach generally has a moderate slope (1:30), often with a single crescentic bar and a steep (1:8) beach face (see Figure 9). The offshore surface elevation in 12-m depth was inferred using pressure sensor measurements. The surface elevations and velocities on a transect from offshore to the shoreline were measured using a pressure sensor and current meters mounted on a movable sled [see *Sallenger*, 1982]. The base of the sled had dimensions of 4 × 5.5 m. A 10-m mast was attached to the base and extended out of the water. The position and elevation of the sled relative to a baseline and MSL were optically surveyed from shore.

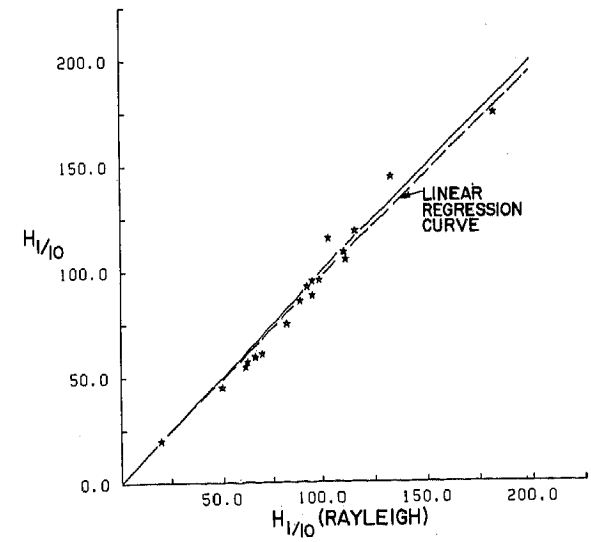

Fig. 7. Measured $H_{1/10}$ plotted against Rayleigh statistic $H_{1/10}$.

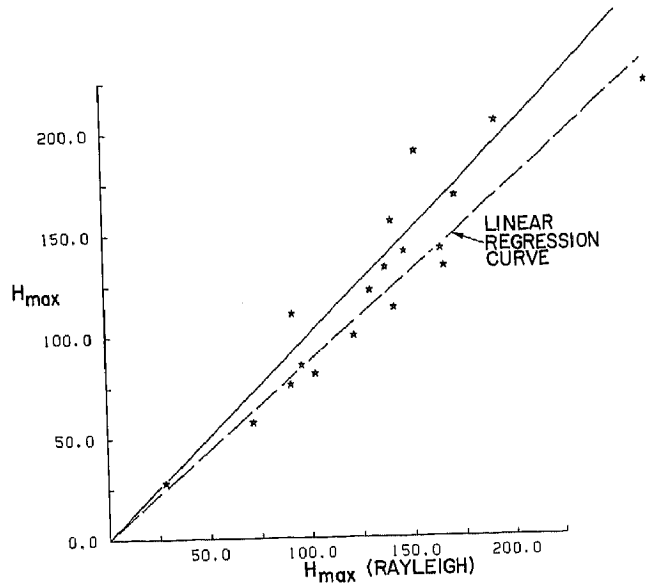

Fig. 8. Measured H_{max} plotted against Rayleigh statistic H_{max}.

The sled was moved using a continuous 'clothes line' arrangement. A 1-inch (2.54 cm) nylon rope was attached to both ends of the sled. The line leading offshore was fed through a block affixed to an anchor in approximately 10-m depth; the line then led back to shore where a winch could pull the sled offshore. The line attached to the shoreward end of the sled was pulled on directly to bring the sled onshore. In this manner the sled could be positioned anywhere on the transect between 10-m depth and the beach.

Measurements were taken at a fixed location for 35 minutes, and then the sled was moved to another location for the next run. Waves visually observed to be breaking or broken as they passed the mast of the sled were electronically flagged and recorded simultaneously with pressure sensor data. The flagged wave heights were measured from the wave record (after having converted the pressure record to surface elevations) using the zero-up-crossing technique to obtain a breaking wave height distribution. Wave height distributions for all waves (including breaking and nonbreaking) and the corresponding breaking wave height distributions (hatched area) for four locations (furthest offshore at the top and proceeding shoreward down the figure) are shown in Figure 10. Since the data were not measured simultaneously but sequentially, the wave height values have been normalized by the offshore rms wave height H_0 to account for any variability in the incident wave conditions. The Rayleigh pdf is superimposed on the measured wave height distribution (solid line) and again appears to represent the wave heights well. The breaking wave height distributions show that even at the 5-m depth, the waves occasionally broke, and it was not always the largest waves that broke.

Since there is no theory for describing breaking wave distributions $p_b(H)$, we simply fit empirical expressions to the observed distributions. In describing $p_b(H)$ three rules will be applied: (1) $p_b(H)$ should resemble the observations (Figure 10), (2) $p_b(H)$ is a subset of the distribution $p(H)$ for all waves, breaking and nonbreaking, and (3) the area under the distribution is equal to the percent of breaking waves; this rule is a convenient definition to keep track of what percent are broken waves and means that $p_b(H)$ is not a pdf.

The distribution of breaking wave heights can be expressed as a weighting of the Rayleigh distribution for all waves:

$$p_b(H) = W(H)p(H) \tag{17}$$

where the weighting function $W(H) \leq 1$, to insure $p_b(H) \leq p(H)$ in accordance with rule (2) above. The integral property ((3) above) is

$$A_b = \int_0^\infty p_b(H)\, dH \tag{18}$$

where A_b is the fraction of all waves which are breaking and that in deep water, $A_b \to 0$ as $h \to \infty$, and in surf zone $A_b \to 1$ as $h \to 0$, i.e., all waves are breaking.

The simplest hypothesis is that the waves break in proportion to the distribution for all waves, so that

$$W(H) = A_b \tag{19}$$

where A_b is independent of H and dimensionless.

Let

$$W(H) = A_b = \left(\frac{H_{rms}}{\gamma h}\right)^n \tag{20}$$

with n a variable to be determined from the observations. The form of (20) is motivated by two considerations. Firstly, the importance of the parameter $H_{rms}/\gamma h$ is expected because of the well-known depth limiting condition for shallow water monochromatic waves, $H = \gamma h$. Secondly, (20) yields analytical solutions for the transformation of H_{rms} on a plane beach.

A problem with (20) is that the likelihood of a wave breaking is independent of its height, since $W(H) =$ constant. Observations show that at a particular location the largest waves are more likely to break. Hence a greater proportion of the larger waves contribute to the breaking wave distribution, resulting in the breaking wave distribution generally being skewed to the higher waves relative to the Rayleigh. The skewing of the observed breaking wave height distributions is obvious in Figure 10.

A simple modification to (20) which more heavily weights the larger waves is given by

$$W(H) = \left(\frac{H_{rms}}{\gamma h}\right)^n \left[1 - \exp\left(-\left(\frac{H}{\gamma h}\right)^2\right)\right] \leq 1 \tag{21}$$

Thornton and Guza [1982] showed that for Torrey Pines in the inner surf zone, an envelope curve relating rms wave height to depth was well approximated by

$$H_{rms} \simeq 0.42\, h \tag{22}$$

A value of $\gamma = 0.42$ was also found for the Soldiers Beach waves and suggests similarity of the breaking wave processes in the inner surf zone at the two sites. Therefore a value of $\gamma = 0.42$ is used.

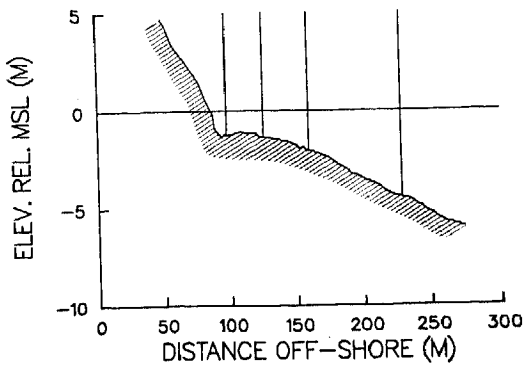

Fig. 9. Beach profile at Soldiers Beach, California on August 24, 1981. Vertical lines indicate measurement locations.

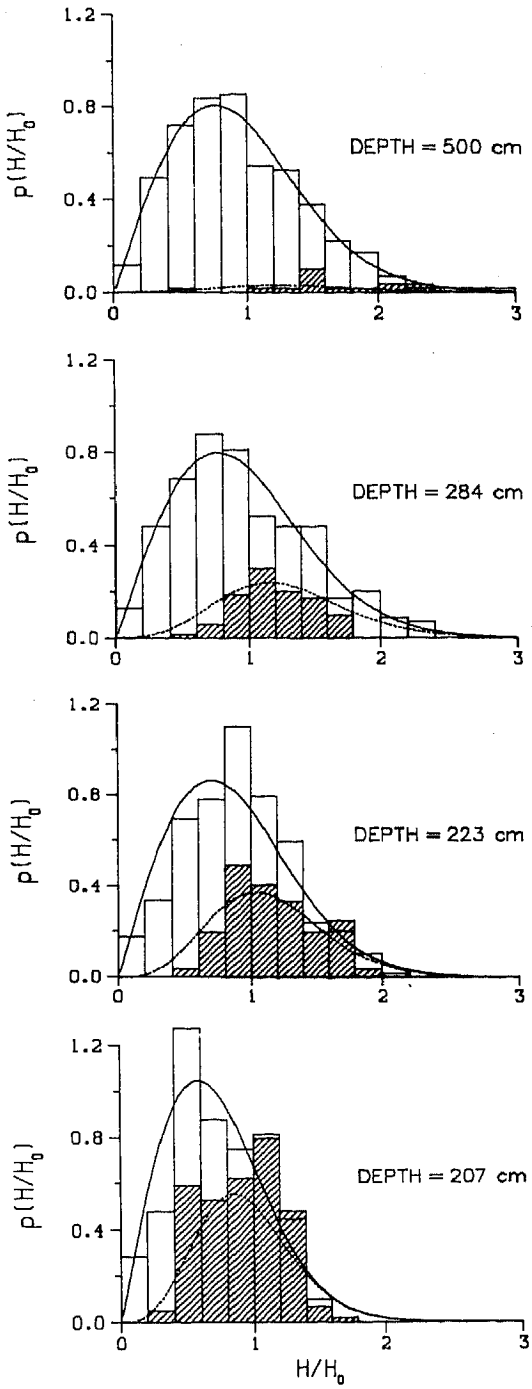

Fig. 10. Wave height distributions and breaking wave height distributions (hatched area) normalized to offshore rms wave height H_0. The Rayleigh distribution is given as a solid line and the empirical breaking wave distribution using (21) is given as a dashed line.

The percentage of breaking waves as a function of $\gamma h/H_{rms}$ described using (20) with $n = 2$ and 4 and using (21) with $n = 2$ are compared with the field measurements (Figure 11). Only a small percent of waves are predicted to break until about $\gamma h/H_{rms} \simeq 2$, after which the waves very quickly reach saturation, at which time all waves are breaking, i.e., $\gamma h/H_{rms} = 1$.

The comparisons in Figure 11 suggest that $p_b(H)$, described by either weighting functions (20) with $n = 4$, or (21), reasonably describes the percent of all waves which are breaking. The shapes of these breaking wave distributions are compared with the measured breaking wave distribution at 2.23-m depth (Figure 12); the $p_b(H)$ for this shape comparison have been adjusted so that their areas are the same as measured. The $p_b(H)$

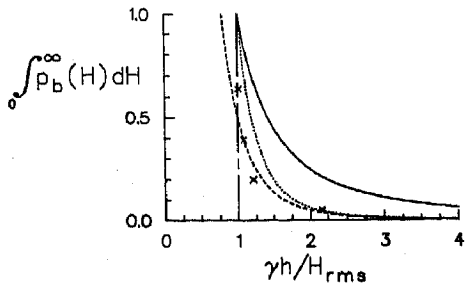

Fig. 11. The percent of breaking waves versus $\gamma h/H_{rms}$ with $\gamma = 0.42$ for $p_b(H)$ specified using (20) with $n = 2$ (solid line), $n = 4$ (dotted line), using (21) (dashed line) and measurements denoted by crosses.

described by (21) appears to give the best fit to the data and has been drawn as a dashed line for all the distributions shown in Figure 10. Equation (21) has no physical justification and is simply a convenient empirical expression which fits the observations. Equation (20) does not fit the data as well but leads to an analytic solution derived in the next section.

The $p_b(H)$ given by (17)–(21) are used to calculate $\langle \varepsilon_b \rangle$ to complete the model description. Note that the Rayleigh pdf is completely specified by H_{rms}, and H_{rms} is calculated by integrating the energy flux equation (8) from deep water to the location of interest.

3.5. *Energy Dissipation*

The energy dissipation is considered primarily due to the conversion of potential wave energy to turbulent kinetic energy, which is eventually lost to heat during wave breaking, and secondarily due to bottom frictional losses. The energy dissipation in a breaking wave is modeled after a periodic bore. The rate of energy dissipation per unit area for each bore using the description for Q given by (7) is

$$\varepsilon_b = \frac{\bar{f}}{4} \rho g \frac{(BH)^3}{h} \tag{23}$$

The average rate of energy dissipation is found by adding up the dissipation for each broken wave calculated using (23) and dividing by the total number of waves (including broken and unbroken waves). In other words, the average rate of energy dissipation is calculated by multiplying the dissipation for a single broken wave of height H by the probability of wave breaking at each height, as given by $p_b(H)$. For the ensemble,

$$\langle \varepsilon_b \rangle = \frac{B^3}{4} \rho g \frac{\bar{f}}{h} \int_0^\infty H^3 p_b(H)\, dH \tag{24}$$

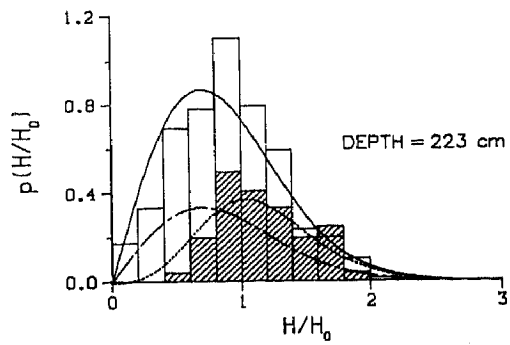

Fig. 12. Wave height and breaking wave height (hatched area) distributions compared with Rayleigh distribution (solid line) and breaking wave distributions using (20) with $n = 4$ (dotted line) and (21) (dashed line). For shape comparisons the areas of empirical breaking wave height distributions have been made equal to measured area.

Two dissipation functions are considered. Substituting $p_b(H)$, described using weighting function (20), with $n = 4$ into (24) and integrating yields

$$\langle \varepsilon_b \rangle = \frac{3\sqrt{\pi}}{16} \rho g \frac{B^3 \bar{f}}{\gamma^4 h^5} H_{\text{rms}}{}^7 \tag{25}$$

Although using this $p_b(H)$ did not give the best fit to the data, its use leads to an analytical solution (described below) which allows us to easily explore the model behavior. The second dissipation function is obtained using (21) to describe $p_b(H)$, giving

$$\langle \varepsilon_b \rangle = \frac{3\sqrt{\pi}}{16} \rho g B^3 \bar{f} \frac{H_{\text{rms}}{}^5}{\gamma^2 h^3} \left[1 - \frac{1}{(1 + (H_{\text{rms}}/\gamma h)^2)^{5/2}} \right] \tag{26}$$

3.6. *Analytical Solution*

An analytical solution in shallow water can be obtained for waves approaching normally on a plane sloping beach. Although the solution is only applicable in shallow water, considerable insight into the workings of the model can be obtained. Starting with the energy flux equation (8) with E described by (9) and describing the bore dissipation using (25) gives

$$\frac{d}{dx} \frac{1}{8} \rho g H_{\text{rms}}{}^2 C_g = \frac{3\sqrt{\pi}}{16} \frac{\rho g \bar{f} B^3}{\gamma^4 h^5} H_{\text{rms}}{}^7 \tag{27}$$

The independent spatial variable can be transformed for a plane sloping beach using

$$x = \frac{h}{\tan \beta} \tag{28}$$

By applying the shallow water linear approximation $C_g \simeq C = \sqrt{gh}$ and defining

$$y = H_{\text{rms}}{}^2 h^{1/2} \tag{29}$$

(27) is rewritten

$$\frac{dy}{dh} = \frac{3}{2} \left(\frac{\pi}{g} \right)^{1/2} \frac{\bar{f} B^3}{\gamma^4 \tan \beta} \frac{y^{7/2}}{h^{27/4}} \tag{30}$$

(30) is easily integrated to give

$$-y^{-5/2} = -\frac{1}{a} h^{-23/4} + \text{const.} \tag{31}$$

where

$$a = \frac{23}{15} \left(\frac{g}{\pi} \right)^{1/2} \frac{\gamma^4 \tan \beta}{B^3 \bar{f}} \tag{32}$$

Since the shallow water approximation was made, the offshore boundary condition is defined where the shallow water approximation becomes valid (within one percent):

$$y = y_0 = H_0{}^2 h_0{}^{1/2} \quad \text{at} \quad h_0 \leq \frac{L}{20} \tag{33}$$

After applying the outer boundary condtion to specify the integration constant, the complete solution for y is

$$y = a^{2/5} [(h^{-23/4} - h_0{}^{-23/4} + y_0]^{2/5} \tag{34}$$

The solution can be stated in terms of the deep water wave conditions by assuming conservation of energy flux and using finite depth linear theory seaward of h_0.

$$y_0 = H_0{}^2 h_0{}^{1/2} = H_d{}^2 \frac{C_{gd}}{g^{1/2}} K_r = \frac{1}{4\pi} H_d{}^2 \frac{g^{1/2}}{\bar{f}} K_r = y_d \tag{35}$$

where the subscript d refers to deep water and K_r accounts for refractive effects. The offshore solution (35) and the shallow water solution (34) are matched at h_0. Transforming back and expressing in terms of wave height:

$$H_{\text{rms}} = a^{1/5} h^{9/10} \left[1 - h^{23/4} \left(\frac{1}{h_0{}^{23/4}} - \frac{a}{y_d{}^{5/2}} \right) \right]^{-1/5} \tag{36}$$

$$0 \leq h \leq h_0$$

The asymptotic case as the depth gets very shallow is

$$H_{\text{rms}} \simeq a^{1/5} h^{9/10} \quad \text{as} \quad h \to 0 \tag{37}$$

which says that the wave height in the inner surf zone is related to the depth and independent of the initial conditions in deeper water. This result is similar to the observations at Torrey Pines Beach [*Thornton and Guza*, 1982] that waves of all initial heights shoaling from deep water become saturated in the inner surf zone with the heights given by (22).

3.7. *Frictional Dissipation*

Frictional dissipation at the bottom boundary layer can easily be included and is described here for completeness but is shown to be a minor dissipation mechanism. Once waves start to break, the average rate of frictional energy dissipation for a single wave is calculated by assuming the usual quadratic formulation for bottom shear stress,

$$\varepsilon_f = \mathbf{v}_h \boldsymbol{\tau}_h = \rho c_f \mathbf{v}_h{}^2 |\mathbf{v}_h| \tag{38}$$

where the h subscript refers to bed and c_f is the bed friction coefficient. Again assuming a very narrow-band wave spectrum so that all waves have the same average period and applying linear theory to describe the wave-induced velocity at the bed, the frictional energy dissipation for a single wave is

$$\varepsilon_f = \rho c_f \frac{1}{6\pi} \left(\frac{2\pi \bar{f}}{\sinh kh} \right)^3 H^3 \tag{39}$$

The expected (average) frictional dissipation for the ensemble (all waves) is calculated using the Rayleigh probability distribution (17), since all waves contribute to the velocities at the bed:

$$\langle \varepsilon_f \rangle = \rho c_f \frac{1}{6\pi} \left(\frac{2\pi \bar{f}}{\sinh kh} \right)^3 \int_0^\infty H^3 p(H)\, dH$$

$$= \rho c_f \frac{1}{16\sqrt{\pi}} \left[\frac{2\pi \bar{f} H_{\text{rms}}}{\sinh kh} \right]^3 \tag{40}$$

Dissipation due to breaking and friction can be compared for the shallow water case ($\sinh kh \simeq 2\pi (hg^{-1})^{1/2} \bar{f}$) within the surf zone using the breaking wave dissipation function (25) and (40)

$$\frac{\langle \varepsilon_f \rangle}{\langle \varepsilon_b \rangle} = \frac{\gamma^4 g^{1/2}}{3\pi \bar{f}} c_f \frac{h^{7/2}}{H_{\text{rms}}{}^4} \tag{41}$$

In the inner surf zone, (37) applies and (41) reduces to

$$\frac{\langle \varepsilon_f \rangle}{\langle \varepsilon_b \rangle} = \frac{c_f}{3} \left[\frac{g^{1/2}}{\pi \bar{f}} \right]^{1/5} \left[\frac{15}{23} \frac{B\gamma^3}{\tan \beta} \right]^{4/5} h^{-1/10} \tag{42}$$

The frictional dissipation is seen to be relatively more important on a milder sloping beach and for lower frequency waves as would be expected. By using $c_f = 0.01$, an accepted nominal value [*Shemdin et al.*, 1977], and values representative for Torrey Pines Beach of $\bar{f} = 0.07$ Hz, $\beta = 0.02$, $\gamma = 0.42$, and $B = 1.0$ (fully developed bores), the frictional dissipation is less than 3% of the dissipation due to breaking for depths greater than 20 cm within the surf zone. Similar comparisons are

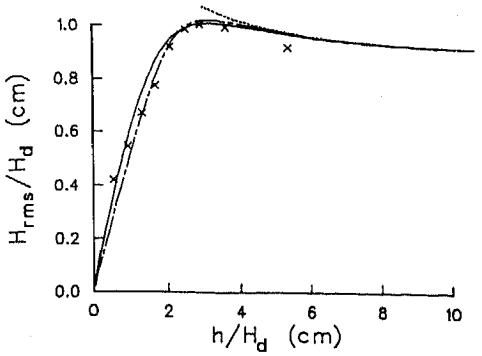

Fig. 13. Model generated H_{rms} versus distance offshore normalized by deep water wave height ($H_d = 12.6$ cm) plotted against laboratory data from *Battjes and Janssen* [1978]. Solid line is M2, upper dashed line is linear wave theory with no dissipation, and dot-dashed line is M1.

obtained for laboratory beaches. The solution indicates that frictional dissipation is negligible compared with the dominant wave breaking dissipation, except in the very shallowest water as $h \to 0$, say, in the run-up region, where the boundary layer effects dominate. Our analysis is not concerned with the run-up region so that frictional dissipation will be neglected.

3.8. *Numerical Model*

For the complete solution starting in arbitrary depth, for general bottom profiles, numerical integration must be used. For the numerical solution the more accurate description of $p_b(H)$, described using (21) resulting in breaking wave dissipation (26), will be employed. The energy flux balance equation (8) is solved by substituting the bore dissipation function (and bottom friction dissipation function) and numerically integrating from offshore to the shoreline. Several numerical schemes were investigated. A fourth-order Runge-Kutta coupled with a fourth-order Adams-Moulton extrapolation scheme [*Gerald*, 1978] was used as a standard. In the end, it was found that the simplest forward stepping scheme is sufficiently accurate, where

$$EC_{gx}|_2 = EC_{gx}|_1 + \langle \varepsilon_b \rangle|_1 \, \Delta x + \langle \varepsilon_f \rangle|_1 \, \Delta x \qquad (43)$$

Starting from the deepest measurement, say, location 1 where $H_{rms,1}$ and $\bar{f}$ are given, the integration and predicted quantities are obtained as follows. $C_{gx}|_{1,2}$ and E_1 are calculated using the linear theory relationships (9) and (10) since $H_{rms,1}$ and h_1 and h_2 are known. The dissipation $\langle \varepsilon_b \rangle|_1$ is calculated using (26) where H_{rms} is calculated at 1. E_2 (and hence $H_{rms,2}$) is then predicted, since this is the only remaining variable. The data have shown the Rayleigh distribution does a good job of describing wave heights everywhere, so the pdf at location 2 is completely specified using the predicted $H_{rms,2}$. The model also predicts the fraction of waves which have broken and their pdf. Further space steppings yield similar predictions at all shoreward locations.

In the application of the model, the coefficient $\gamma = 0.42$ has been applied as determined from the data. The only undetermined coefficient then is B, which is found by model fitting. B and γ could have been combined into one coefficient to be determined from the data, but it was felt that greater insight is retained by treating them separately. It is expected that $B = 0(1)$ if the model is performing properly.

4. MODEL COMPARISONS

4.1. *Laboratory Data*

The numerical energy flux balance model was run using dissipation functions (25) and (26), denoted models M1 and M2 respectively. The results, along with the curve for no dissipation, i.e., energy is conserved, are compared with laboratory data from *Battjes and Janssen* [1978] (Figure 13). Only the portion of the curve near the beach is shown. The lab data were measured on a 1:20 beach slope; the generated waves were random, with mean frequency of 0.407 Hz and a deep water rms wave height H_d of 12.6 cm. The waves broke as plunging breakers. The waves were one-dimensional in the laboratory channel so that $C_{gx} = C_g$ in (10). A γ value of 0.4 was measured from Figure 13. Model fitting suggests that $B = 0.8$ is reasonable for both models. For the same B value, model M2 is more dissipative. This is expected because the breaking wave distribution using weighting function (21) in M2 is skewed to higher waves relative to that for M1. Thus when taking high moments to calculate the breaking wave dissipation as in (25), M2 dissipation will be greater.

The departure of the model results from the measured lab values at the shallowest depths is partly because the model does not account for wave set-up. It is clear that increasing the mean depth with set-up would increase the theoretical H_{rms}, bringing the inner surf zone data into closer agreement with the model results.

The analytical solution is not applied to the plane sloping laboratory beach because the shallow water solution is not applicable until the depth is 15 cm ($h/H_d = 1.2$ in Figure 13) for the short, 2.5-s-period waves. However, the analytical model does have application to the field. For example, for the relatively long-period waves incident at Torrey Pines Beach with mean period ranging between 13 and 18 s, the corresponding shallow water depth limits are 4 and 8 m.

4.2. *Model Comparisons with Field Data*

For comparison purposes the bottom contours at Torrey Pines can be considered straight and parallel and the waves normally incident. *Guza and Thornton* [1980] performed refraction and shoaling sensitivity model testing using linear refraction. Waves of 0.067 Hz and varying angle of incidence from 0° to ±15° were refracted from 10- to 3-m depth using the measured bathymetry at Torrey Pines Beach. The tests showed the percent difference between linearly shoaled wave heights (within the 15° angular spread) on the measured topography and normally incident waves on plane parallel contours was less than 5% for any directional band. Therefore the waves can be approximated as normally incident and shoaled over the measured bathymetry on the instrument transect. This simplifies the analysis, since $C_{gx} = C_g$ in (8).

The model M2 is compared with the 6 days of data representing a relatively broad range of wave conditions (see Table 2). Optimal model coefficients B determined by iteration were sought to represent individual days and also a single value was sought to represent all days. The sums of the square error of the model H_{rms} compared with the measured H_{rms} were calculated

TABLE 3. Optimal B values for Model M2

Date	B	Percent Error	Number of Instruments
Nov. 4	1.5	7.3	16
Nov. 10	1.7	5.3	12
Nov. 12	1.3	7.0	8
Nov. 17	1.5	7.9	14
Nov. 18	1.5	9.3	12
Nov. 20	1.6	6.3	12
All days	1.5	8.6	74
Lab	0.8	6.1	9

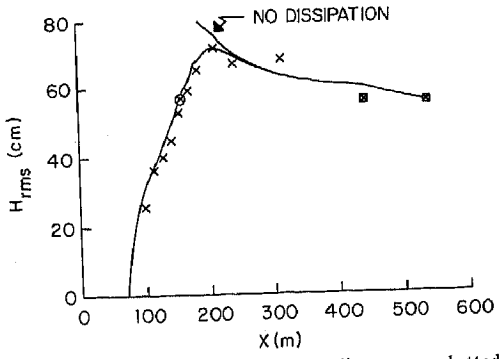

Fig. 14. Model generated H_{rms} versus distance x plotted against measured values for November 10, 1978. Solid line is M2 without friction, upper solid line is linear wave theory with no dissipation. The measured H_{rms} values were determined from sea surface elevations measured directly with a wave staff (circle) and by applying linear theory to the velocity (crosses) and pressure (squares) measurements to infer sea surface elevations.

for all sensors for each of 6 days and for all 6 days using various values of B. The optimal values of B, the number of instruments, and the standard error compared with the field data are given in Table 3. The value of B obtained for the laboratory data of *Battjes and Janssen* [1978] is also given. Since most of the instruments were located from just outside the surf zone to the beach, B is weighted to fit the data better in this region; this also coincides with the zone in which most of the dissipation and change occur.

Model M1 was also run and an optimal value was found for $B = 1.72$ with a standard error of 8.3% for all days. Even though model M1 gives a slightly less error than M2, the latter is the preferred model because the breaking wave distribution used appears to be more appropriate (Figure 12). Therefore model M2 will be used to demonstrate the data comparisons.

Examples of model M2 comparisons with measurements for the 10th and 20th of November are shown in Figures 14 and 15. A value of B equal to 1.5, the average for all days, has been used. Using optimal B values for the particular days given in Table 3 would give slightly better fits, particularly in the nearshore region. The waves on November 10 were relatively broadbanded sea while the waves on November 20 were very narrow-banded swell. A comparison with conservation of energy for linear waves outside the surf zone is shown for November 10; the difference between the model and conservation of energy is slight until very near the surf zone.

For November 20 the model was run with and without dissipation due to friction. Adding bed friction dissipation by using a uniform bed shear stress coefficient c_f equal to 0.01 resulted in a maximum additional decrease in wave height about the mean breaker line of less than 3% which is consistent with our earlier analysis. Again, because frictional dissipation is of secondary importance and complicates the analysis by introducing another unspecified coefficient, it is not included in the final results.

Figures 14 and 15 show that the model is capable of predicting the wave height increase due to shoaling and subsequent decrease due to wave breaking. The waves peak up to a maximum, a point defined here as the mean breaker line, and then decreases. In the inner surf zone, all the waves become locally depth controlled, and changes in the depth are reflected in changes in wave height. The 'wiggles' in the results in the inner surf zone for November 20 (Figure 15) are due to variations in the bottom profile.

All the measured H_{rms} versus model predicted values are shown in Figure 16. The model results do not appear to depend on the magnitude of H_{rms}, i.e., as the wave height increases, the differences from the 45° line do not increase. The percentage error between predicted and measured H_{rms} plotted against distance offshore (Figure 17) shows that the model predicted H_{rms} values are within ±20% of the measured values and usually much less. The error standard deviation (standard error) is 0.086.

H_{rms} measurement errors are due to sensor errors and errors inherent in transforming the velocity and pressure measurements to surface elevations with linear wave theory. The current meter and pressure sensor calibration errors were of the order of ±5%. The combined error associated with linear theory and sensor error is less than ±20% [see *Guza and Thornton*, 1981, Figure 5], which is not substantially different from the error between model and measurements. Therefore much of the difference between model and measurements could be due to measurement errors.

4.3. *Discussion*

Why does the model seemingly work so well while incorporating a number of grossly simplifying assumptions? The basic ingredients making up the model are the energy flux equation and a bore dissipation function. The energy flux balance equation (8) is a correct statement of the physics, but the linearized theory is only valid to the first order in nonlinearity, which is certainly of questionable accuracy near breaking. Even so, the conservation of linearized energy flux (no dissipation) was shown to do a good job of predicting the shoaling of H_{rms} until very near the surf zone, both in the lab (Figure 13) and in the field at Torrey Pines Beach (Figure 14 and *Guza and Thornton* [1980]).

The model predicts wave saturation conditions in the inner surf zone where the wave height is strongly a function of the depth. It is difficult to discriminate between the $h^{9/10}$ dependence on H_{rms} in the inner surf zone predicted by the analytical model and the linear dependence suggested by *Thornton and Guza* [1982] using the data. The difference between the two curves is not significant over the interval of measured wave heights in the inner surf zone (100- to 15-cm depth), given the scatter of data.

Since the predictions of H_{rms} using the models describing $p_b(H)$ in two different ways gave essentially the same results, it is concluded the model results are not strongly sensitive to the forms of $p_b(H)$. The differences in $p_b(H)$ are compensated for by using different values of B.

The accuracy of the model is dependent on the selection of B.

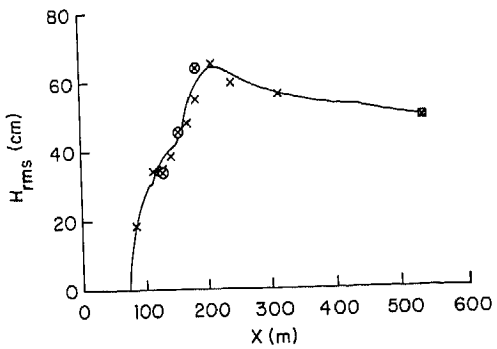

Fig. 15. Model M2 generated H_{rms} versus x plotted against measured values for November 20, 1978. The measured H_{rms} were determined from sea surface elevations measured using wave staffs (circles) and by applying linear theory to the velocity (crosses) and pressure (squares) measurements to infer sea surface elevations.

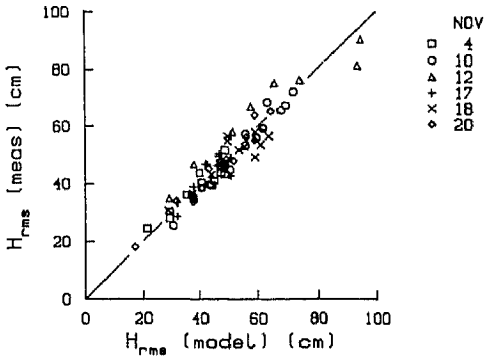

Fig. 16. H_{rms} measured versus H_{rms} model.

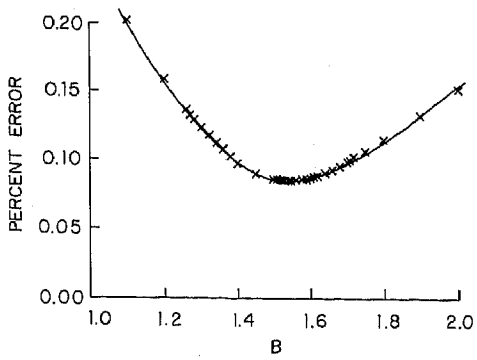

Fig. 18. Model M2 error prediction compared with Torrey Pines data for all days for various values of B.

For the two very different applications of the model M2 to the field and lab data, B values of 1.54 (average for all 6 days) and 0.8 were obtained. Since parameter B represents the percentage of foam on the face of the wave, which is a measure of the intensity of breaking, it is expected B would depend on the breaking wave characteristics, but no such correlation was found, which is apparent by comparing B with various wave parameters in Tables 2 and 3.

The sensitivity of the model to the selection of B used for all days is shown in Figure 18, where various values of B are plotted against standard error. The curve shows that a variation of $\pm 25\%$ about the optimal value B results in an increased model error of less than 10%. Therefore the model fit to data is not overly sensitive to the slection of B.

The condition $B \leq 1.0$ is expected on physical grounds, with $B = 1$ corresponding to fully developed bores. Since $\langle \varepsilon_b \rangle$ is proportional to B^3 in (23), the result that the optimal value of $B = 1.54$ implies the simple periodic bore dissipation function underestimates the dissipation by almost a factor of four. However, from Figure 18, using a B value of 1.2 would only slightly degrade the model fit and result in only a 70% underestimation. *Stive* [1983] made detailed measurements of breaking wave disipation for monochromatic waves breaking on a gently sloping (1:40) plane laboratory beach. He concluded from an evaluation of laser doppler flow field measurements that there was a strong resemblance between the internal mean and turbulent flow fields of quasisteady breakers, bores, and weak hydraulic jumps. But he found that the classical periodic bore formulation, as used in this analysis, underestimated the measured dissipation rates by 30% to 50%. This laboratory result is qualitatively consistent with the field results.

As mentioned earlier, various other forms for the bore dissipation function have been suggested. Several of these other dissipation forms were investigated, but it was decided that the physical rationale for using these other bore dissipation functions was not justified on the basis of the data presently available. Therefore the simplest physical model has been presented and compared with data.

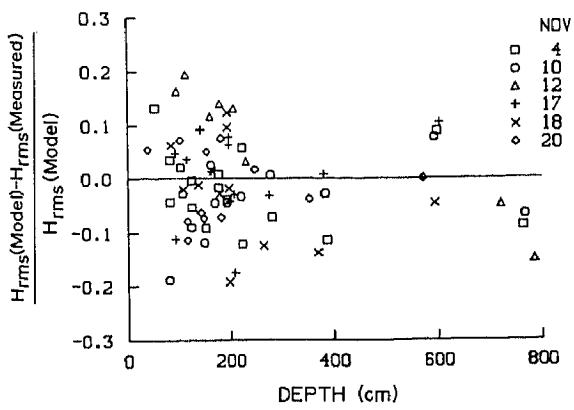

Fig. 17. Percent error between model and measured H_{rms} as a function of distance offshore.

5. Summary and Conclusions

The Rayleigh distribution is shown to give surprisingly good estimates of wave height statistics, even H_{max}, for the spilling breakers measured at Torrey Pines Beach. The percent mean errors over the measured ranges compared with the Rayleigh statistics of $H_{1/3}$, $H_{1/10}$, and H_{max} were -0.2, -1.8, and -6.8%, respectively. The results show the Rayleigh distribution to slightly overpredict the number of waves in the tail of the distribution, but it is nevertheless able to predict the central statistics of $H_{1/3}$ and even $H_{1/10}$ well.

A model describing the transformation of random wave heights was developed based on energy flux balance. Dissipation is considered due to wave breaking and bed friction. Wave breaking is characterized after periodic bores. The random nature of the wave heights is described using the Rayleigh distribution everywhere, as suggested by the data. An empirical breaking wave height distribution based on the field data is used to define which waves the bore dissipation function is applied. The model is capable of predicting the increase in averaged wave height due to shoaling and subsequent decrease due to wave breaking. Bottom friction dissipation using $c_f = 0.01$ results in a maximum wave decrease of 3% occurring about the mean breaker line compared with the inviscid shoaling. Because it is of secondary importance and introduces a second unspecified coefficient, bed friction is not included. The model has only one adjustable parameter, B, which is a measure of the intensity of wave breaking.

The model is compared both with laboratory data and the extensive set of field measurements collected at Torrey Pines Beach, California. The model is able to predict rms wave heights to within a standard error of 8.6% throughout the region from offshore to the beach. Although good comparisons are obtained, the results suggest simple bore theory underestimates the dissipation. The underestimates are compensated by adjusting the B coefficient.

Acknowledgments. This work was supported by the Office of Naval Research, Coastal Sciences Branch, under contract numbers NR 388-114 (for E. B. Thornton) and N00014-75-C-0300 (for R. T. Guza), the National Science Foundation under contract number DAR-8023425 (for E. B. Thornton), and the Sea Grant Nearshore Sediment Transport Study (project number R/CA-N-4D). R. J. Seymour obtained the bathymetric data. The staff of the Shore Processes Laboratory (Scripps

Institution of Oceanography) installed and maintained the offshore sensors and data acquisition system. R. L. Lowe was the principal engineer. A. Sallenger and his crew at the U.S. Geological Survey are thanked for their cooperation in obtaining the breaking wave distributions. D. O. Burych aided substantially in the data processing. A critical review by J. A. Battjes, which lead to an improvement in the model, is gratefully acknowledged.

REFERENCES

Battjes, J. A., Set-up due to irregular waves, in *Proceedings of the 13th International Conference Coastal Engineering*, pp. 1993–2004, American Society of Civil Engineers, New York, 1972.

Battjes, J. A., and J. P. F. M. Janssen, Energy loss and set-up due to breaking of random waves, in *Proceedings of the 16th International Conference Coastal Engineering*, p. 569, American Society of Civil Engineers, New York, 1978.

Bowen, A. J., D. L. Inman, and V. P. Simmons, Wave 'set-down' and wave set-up, *J. Geophys. Res.*, *73*, 2569–2577, 1968.

Cartwright, D. E., and M. S. Longuet-Higgins, The statistical distribution of the maxima of a random process, *Proc. R. Soc. London Ser. A*, *237*, 212–232, 1956.

Collins, J. I., Probabilities of breaking wave characteristics, in *Proceedings of the 13th International Conference Coastal Engineering*, pp. 399–412, American Society of Civil Engineers, New York, 1970.

Chakrabarti, S. K., and R. P. Cooley, Statistical distributions of periods and heights of ocean waves, *J. Geophys. Res.*, *82*, 1363–1368, 1977.

Forristall, G. Z., On the statistical distribution of wave heights in a storm, *J. Geophys. Res.*, *83*, 2353–2358, 1978.

Gerald, C. F., *Applied Numerical Analysis*, Addison-Wesley, 1978.

Goda, Y., A synthesis of breaker indices (in Japanese), *Trans. Jpn. Soc. Civ. Eng.*, *13*, 227–230, 1970.

Goda, Y., Irregular wave deformation in the surf zone, *Coast. Eng. Jpn.*, *18*, 13–26, 1975.

Guza, R. T., and E. B. Thornton, Local and shoaled comparisons of sea surface elevations, pressures, and velocities, *J. Geophys. Res.*, *85*, 1524–1530, 1980.

Guza, R. T., and E. B. Thornton, Wave set-up on a natural beach, *J. Geophys. Res.*, *86*, 4133–4137, 1981.

Huntley, D., R. T. Guza, and E. B. Thornton, Field observations of surf beat, 1, Progressive edge waves, *J. Geophys. Res.*, *86*, 6451–6466, 1981.

Hwang, L.-S., and D. Divoky, Breaking wave set-up and decay on gentle slopes, in *Proceedings of the 12th International Conference Coastal Engineering*, pp. 377–389, American Society of Civil Engineers, New York, 1970.

Kuo, C. T., and S. T. Kuo, Effect of wave breaking on statistical distribution of wave heights, *Proc. Civ. Eng. Oceans*, *3*, 1211–1231, 1974.

LeMehauté, B., On non-saturated breakers and the wave run-up, in *Proceedings of the 8th International Conference Coastal Engineering*, pp. 77–92, American Society of Civil Engineering, New York, 1962.

LeMehauté, B., and R. C. Y. Koh, On the breaking of waves arriving at an angle to the shore, *J. Hydraul. Res.*, *5*(1), 541–549, 1967.

Longuet-Higgins, M. S., On the statistical distribution of the heights of sea waves, *J. Mar. Res.*, *11*(3), 245–266, 1952.

Longuet-Higgins, M. S., On the joint distribution of the periods and amplitudes of sea waves, *J. Geophys. Res.*, *80*, 2688–2694, 1975.

Longuet-Higgins, M. S., On the distribution of the heights of sea waves: Some effects of nonlinearity and finite bandwidth, *J. Geophys. Res.*, *85*, 1519–1523, 1980.

Miche, R., Mouvements ondulatoires des mers en profoundeur constante ou decroissante, *Ser. 3, Issue 363*, Wave Res. Lab., Univ. Calif. at Berkeley, 1954.

Miller, R. L., Role of vortices in surf zone prediction: Sedimentation and wave forces, beach and nearshore sedimentation, *Spec. Publ. 24*, Soc. of Econ. Paleontol. and Minerals, Washington, D.C., 1976.

Pawka, S. S., D. L. Inman, R. L. Lowe, and L. Holmes, Wave climate at Torrey Pines Beach, Calif., *Tech. Pap. 76-5*, Coast. Eng. Res. Center, Fort Belvoir, Va., 1976.

Sallenger, A. H., Jr., P. C. Howard, C. H. Fletcher, III, and P. A. Howd, Profile, wave and current measurement system for the high energy nearshore, *J. Mar. Geol.*, in press, 1983.

Shemdin, O. H., K. Hasselman, S. V. Hsiao, and K. Herterich, Nonlinear and linear bottom interaction effects in shallow water, in *Turbulence Fluxes through the Sea Surface, Wave Dynamics and Prediction*, edited by A. Favre and K. Hasselmann, pp. 347–372, Plenum, New York, 1978.

Shuto, N., Nonlinear long waves in a channel of variable section, *Coast. Eng. Jpn.*, *17*, 1–12, 1974.

Stive, M., Energy dissipation in waves breaking on gentle slopes, *J. Coast. Eng.*, in press, 1983.

Stoker, J. J. *Water Waves*, Interscience, New York, 1957.

Tayfun, M. A., Narrow-band nonlinear sea waves, *J. Geophys. Res.*, *85*, 1548–1552, 1980.

Tayfun, M. A., Breaking-limited wave heights, *J. Waterw., Port, Coast Ocean Div. Am. Soc. Civ. Eng.*, *107*(WW2), 59–70, 1981.

Thornton, E. B., and R. T. Guza, Energy saturation and phase speeds measured on a natural beach, *J. Geophys. Res.*, *87*, 9499–9508, 1982.

(Received October 9, 1981;
revised March 25, 1983;
accepted March 28, 1983.)